


# East Asian winter monsoon variation during the last 3000 years as recorded in a subtropical mountain lake, northeastern Taiwan

The Holocene  
2021, Vol. 31(9) 1430–1442  
© The Author(s) 2021  
Article reuse guidelines:  
sagepub.com/journals-permissions  
DOI: 10.1177/09596836211019094  
journals.sagepub.com/home/hol  


Tsai-Wen Lin,<sup>1</sup>  Stefanie Kaboth-Bahr,<sup>2</sup> Kweku Afrifa Yamoah,<sup>3</sup>  
André Bahr,<sup>4</sup> George Burr,<sup>1</sup>  Yuan-Pin Chang,<sup>5</sup>   
Elisabeth Dietze,<sup>6</sup> Hong-Chun Li,<sup>1</sup> Chih-Chieh Su,<sup>7</sup>   
Rita SW Yam<sup>8</sup> and Ludvig Löwemark<sup>1</sup>

## Abstract

The East Asian Winter Monsoon (EAWM) is a fundamental part of the global monsoon system that affects nearly one-quarter of the world's population. Robust paleoclimate reconstructions in East Asia are complicated by multiple sources of precipitation. These sources, such as the EAWM and typhoons, need to be disentangled in order to understand the dominant source of precipitation influencing the past and current climate. Taiwan, situated within the subtropical East Asian monsoon system, provides a unique opportunity to study monsoon and typhoon variability through time. Here we combine sediment trap data with down-core records from Cueifong Lake in northeastern Taiwan to reconstruct monsoonal rainfall fluctuations over the past 3000 years. The monthly collected grain-size data indicate that a decrease in sediment grain size reflects the strength of the EAWM. End member modelling analysis (EMMA) on sediment core and trap data reveals two dominant grain-size end-members (EMs), with the coarse EM 2 representing a robust indicator of EAWM strength. The downcore variations of EM 2 show a gradual decrease over the past 3000 years indicating a gradual strengthening of the EAWM, in agreement with other published EAWM records. This enhanced late-Holocene EAWM can be linked to the expansion of sea-ice cover in the western Arctic Ocean caused by decreased summer insolation.

## Keywords

East Asian Winter Monsoon (EAWM), end member modelling analysis, grain size, late-Holocene, sediment trap

Received 3 May 2020; revised manuscript accepted 15 April 2021

## Introduction

The East Asian Winter Monsoon (EAWM) system is an important sub-component of the global climate system contributing substantially to tropical and subtropical rainfall at a regional scale. Seasonally, the onset of the EAWM is driven by the development of a high-pressure system above Siberia. Cold air outbreaks emanating from the Siberian High during winter periods is a characteristic feature of the EAWM (Zhang et al., 1996). On interannual to decadal time scales, the EAWM shows strong spatial-temporal variability mainly attributed to changes in external forcing such as the El Niño-Southern Oscillation (ENSO) and Arctic sea ice (Guo et al., 2014; Zhang, 2015). Typically, warm (cold) ENSO events are argued to lead to an anomalous lower-tropospheric anticyclone (cyclone) around the Philippines via Gill-type Rossby wave responses in their peak winters that initiate a weak (strong) EAWM (Wang et al., 2000; Zhang et al., 1996). On the other hand, an increase of sea-ice cover in the western Arctic Ocean under low solar irradiance leads to enhanced albedo, together with a significant strengthening of the Siberian High and a deepening of the East Asian trough. This process induces cooling in mid-latitude Asia and therefore strengthens the EAWM, and vice versa for low sea-ice cover conditions (Chen et al., 2014; Wu et al., 2006; Zhang et al., 2015).

According to the fifth Intergovernmental Panel on Climate Change (IPCC) report, climate change is predicted to strongly affect future drought scenarios in the East Asian monsoon region (IPCC, 2014). Particularly, fluctuations in the EAWM have profound effects on the agricultural, economic and societal welfare of ~2.3 billion people living in eastern and south-eastern Asia (Clift and Plumb, 2008; Fu, 2003; Lau and Li, 1984; United

<sup>1</sup>Department of Geosciences, National Taiwan University, Taiwan, ROC

<sup>2</sup>Institute for Geosciences, University of Potsdam, Germany

<sup>3</sup>School of Geography, Earth & Environmental Sciences, University of Birmingham, UK

<sup>4</sup>Institute of Earth Sciences, Heidelberg University, Germany

<sup>5</sup>Department of Oceanography, National Sun Yat-Sen University, Taiwan, ROC

<sup>6</sup>Alfred Wegener Institute for Polar and Marine Research, Polar Terrestrial Environmental Systems, Germany

<sup>7</sup>Institute of Oceanography, National Taiwan University, Taiwan, ROC

<sup>8</sup>Department of Bioenvironmental Systems Engineering, National Taiwan University, Taiwan, ROC

## Corresponding author:

Ludvig Löwemark, Department of Geosciences, National Taiwan University, Taipei, Taiwan, ROC.

Email: ludvig@ntu.edu.tw

Nations, 2019). Sun and Yang (2012) showed that fluctuations in the EAWM in southern China in 2011 led to a severe drought which cost about 1.09 billion dollars in economic losses. According to the fifth IPCC report, climate change is predicted to strongly affect future drought scenarios in the East Asian monsoon region (IPCC, 2014). Yet, the underlying mechanisms driving the EAWM and possible teleconnections over multiple timescales remain poorly understood. This can be partly attributed to scarce paleoclimate records that reflect EAWM variability and/or a lack of appropriate proxies to constrain the EAWM signal. Indeed, proxies used to reconstruct past EAWM variability may be recording other aspects of the hydrological cycle such as humidity and temperature.

A region that is particularly sensitive to EAWM variability is northern Taiwan as it is situated at the southernmost delineation of the EAWM sphere of influence. A compilation of Taiwan's (including our study area) hydroclimate over the mid-Holocene has revealed inconsistencies with climate interpretations in relation to EAWM variability from sedimentary records within the same lakes, as well as from different lakes in northeastern Taiwan. A case in point, during the Little Ice Age (LIA; 550 and 250 year BP) (Mann et al., 2009), the EAWM has been proposed to be weakened (Yang et al., 2020). Based on climatic models this would have led to reduced precipitation across northern Taiwan (Yang et al., 2020) which is in line with pollen-based precipitation reconstructions from our study site Cueifong Lake (Wang et al., 2015). In contrast, the hydroclimate reconstruction from Duck pond (Chen et al., 2008), Lake Kiwulan (Lin, 2004) and Sonlou Lake (Liew et al., 2014), also based on pollen assemblages, show a wet climate during the LIA. While this ambiguity could potentially be linked to discrepancies in the age models, it is more likely due to the lack of incorporating the fundamental processes of sedimentation in the lacustrine systems, which affects the proxy interpretations of the climate reconstructions. Because lakes vary in their catchment and hydrological properties, it is challenging to infer a single mechanism to explain the sedimentation characteristics of records derived from different lakes (Cohen, 2003; Liu et al., 2016). It is therefore of particular importance to understand how the hydrology and sedimentation dynamics in a particular lake are influenced by heavy precipitation events, such as typhoons, as well as by the evaporation-precipitation balance during winter and summer. Such knowledge is crucial to provide a robust interpretation of proxy records and might help to better understand incoherent climate signals preserved in regional proxy records. By observing monthly sediment variation, the factors controlling the physical and geochemical parameters of sediments can be distinguished, and therefore a robust paleoclimate reconstruction can be achieved.

This study aims at reconstructing late-Holocene EAWM fluctuations based on sedimentary records from Cueifong Lake located in northeastern Taiwan. For our analysis we follow a two-stage approach: firstly, we analysed the grain-size distribution of the monthly sediment input into Cueifong Lake during a 2-year period (2017–2019) to understand the modern sedimentation processes. Subsequently, we applied our modern findings to a sediment core from the centre of Cueifong Lake that encompasses the past ~3000 years. The analysis of the monthly grain size changes as well as the grain size distribution in the sediment core were achieved by applying end member modelling analysis (EMMA) (e.g. Dietze et al., 2012, 2014; Weltje et al., 2015). In addition above, we utilized *n*-alkane chain length distributions which have been used extensively to reconstruct hydroclimate fluctuations (Bingham et al., 2010; Nichols et al., 2006; Zhou et al., 2010). Our results will shed new light on (i) the possible mechanisms that affect sediment input into a subtropical mountain lake, (ii) the relationship between modern sediment input variability and the sediment variability recorded in a sediment core covering the

late-Holocene time interval and (iii) linking the recorded sediment fluctuations to climate changes in the late-Holocene and to identify the driving mechanisms.

## Study area

### *Location and catchment characterization*

Cueifong Lake is located 1840 m above sea level in the Taiping Mountains, northeast Taiwan (24°30' N, 121°36' E) (Figure 1a and b). It is situated in a small endorheic basin with a catchment area of 1.32 km<sup>2</sup>. The lake water budget relies on precipitation, runoff and groundwater infiltration (Wang et al., 2015); while its drainage is affected by evaporation and leakage through the bedrock slate layers into the groundwater reservoir (Mao, 2006). Consequently, both the lake area and the lake level are strongly influenced by the seasonal precipitation amount within the catchment area (Lin et al., 2018; Mao, 2006). The lake area ranges between 0.11–0.25 km<sup>2</sup>, and the water level of Cueifong Lake differs by ~4 m between the low lake level season (January–April) and the high lake level season (September–November) (Mao, 2006). During our observation period from September 2017 to December 2019, the average lake level was 4.85 m, with the lowest level at 2.93 m and highest level at 10.14 m.

The bedrock encompassing Cueifong Lake belongs to the Nansuao Formation of Eocene to Oligocene age (56–23 Ma). The Nansuao Formation consists of alternating slate, metaconglomerate and metasandstone (Lin and Lin, 1995). A series of NE-SW striking thrust faults are recognized in the Taiping Mountain region. The nearest fault to Cueifong Lake is the Tsueyfenghu thrust fault, which is located approximately 1 km northwest of the lake (Lin and Lin, 1995).

### *Climatic setting*

Taiwan's climate is controlled by both the East Asian Summer Monsoon (EASM) and East Asian Winter Monsoon (EAWM) systems, as well as seasonal typhoons (Brand and Brelloch, 1974; Chen and Chen, 2003) (Figure 1a). Based on the precipitation characteristic and the sources, the rainfall regime of Taiwan can be divided into five periods: (i) winter (December to February, affected by EAWM), (ii) spring transition (March to April, EAWM transform to EASM), (iii) Mei-yu rains (May to June, EASM-impacted), (iv) typhoon (July–August) and (v) autumn (September–November, EASM transition to EAWM). Early summer Mei-yu rains, in particular, are controlled by the convergence of southward migrating cold air masses from Siberia and northward migrating warm air masses from the Pacific, bringing precipitation to the entire Taiwan island (Chen and Chen, 2003). The rainfalls in autumn and winter are typically brought by the EAWM, which mostly affects northern, northeastern and eastern Taiwan (Chen and Chen, 2003; Chen and Huang, 1999; Yen and Chen, 2000). Three to four typhoons impact Taiwan during the summer months from July to September every year, bringing intense rainfall that lasts 16 h on average, and can produce up to 2000 mm of precipitation at a specific location (Hsu et al., 2013; Shieh et al., 1998). Large volumes of annual rainfall (2221 mm/year in lowland areas, 3858 mm/year in mountain areas) contribute to high erosion and sedimentation rates (~5.2 mm/year), which can result in high-resolution sedimentary records (Central Weather Bureau, 2009; Dadson et al., 2003).

Monthly averaged climatology data from the Taiping Mountain station (located ~8 km west of Cueifong Lake) during 1996–2016 show that the highest monthly mean temperature occurs in July (17.8°C), and the low monthly mean temperature (5.8°C) occurs in January (Figure 1c). Precipitation increases between July and October, overlapping with the typhoon season (July–September) and the autumn-winter precipitation season (September to

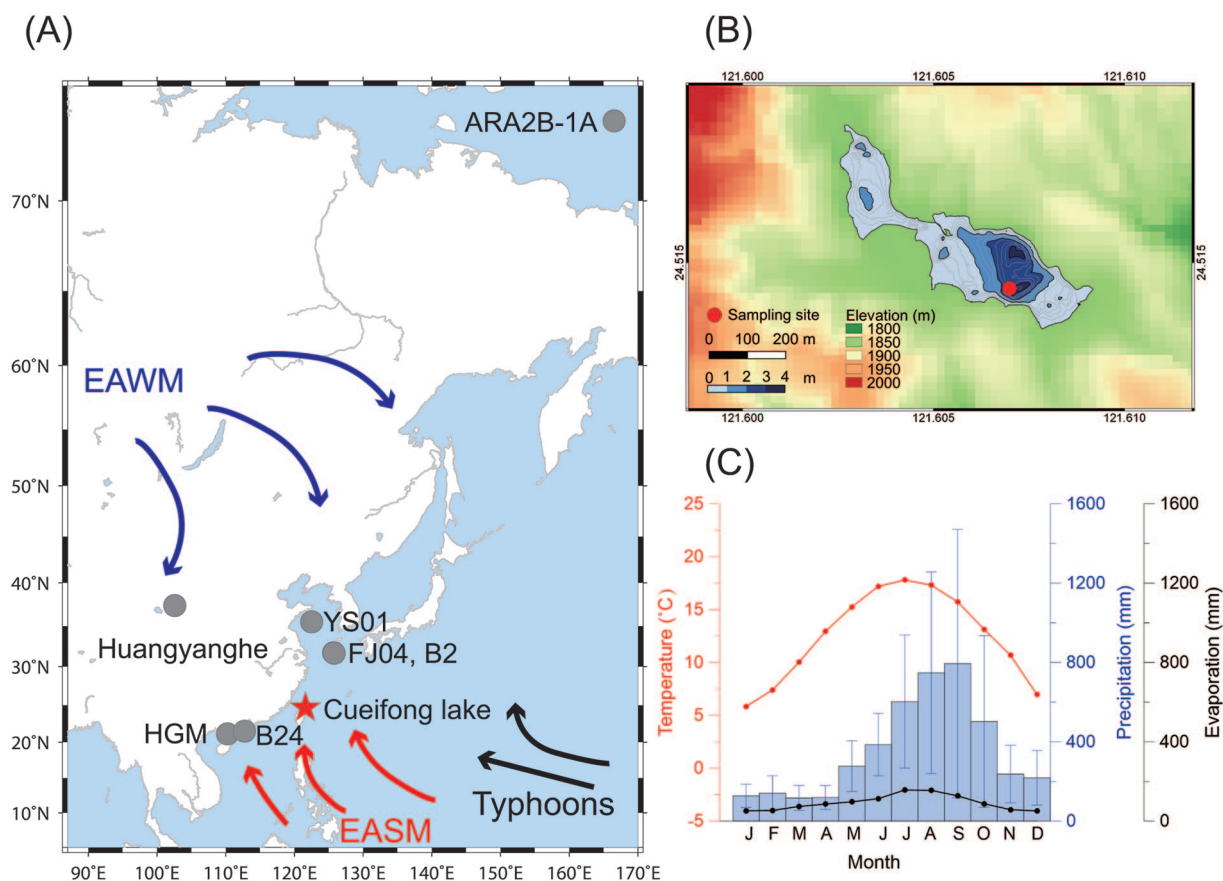


**Figure 1.** (A) Climatic systems affecting the precipitation regime of Taiwan: East Asian winter monsoon (EAWM, blue arrows), East Asian summer monsoon (EASM, red arrows) and typhoons (black arrows). The red star shows the location of Cueifong Lake. Grey dots indicate the geographical position of other EAWM proxy records and the sea-ice coverage record referenced in the text (see also Table 2). (B) Bathymetric map of Cueifong Lake. The red point represents the sampling point of both sediment core and monthly collected sediment (sediment trap). Bathymetry data from a survey conducted on 29 September 2017. (C) Monthly average precipitation (blue bars) and temperature (red line) at Taiping Mountain station during 1996–2016 (Data source: Central Weather Bureau, Taiwan). Monthly average evaporation (black dots) at Yilan station during 1937–1945 (Data source: Academia Sinica, Taiwan).

February). According to climate data collected during 1996–2016 (Central Weather Bureau, 2009), the lake received a mean of 4267 mm precipitation per year, with 898 mm during the interval between March and June (summer monsoon and Mei-yu impacted seasons), 2144 mm during the interval between July and September (typhoon season) and 1224 mm during the interval from October to February (autumn-winter precipitation seasons).

## Materials and methods

### Sediment sampling and lake monitoring

The monthly sediment input into Cueifong Lake was assessed between September 2017 and December 2019 by a set of sediment traps. The design of the sediment traps followed the description of Yang et al. (2011), with slightly modified height and diameter of the trap tubes (15 cm in diameter, 30 cm in height for each tube; four tubes as a trap set). The trap was deployed in the deepest basin of Cueifong Lake (Figure 1b). The tubes were changed at monthly intervals. After filtering the overlying lake water from the sample tube, the sediment was freeze-dried. In addition, a 1.85 m long sediment core (CFL-3) was retrieved in September 2017 using a steel Russian corer in the vicinity of the sediment trap position (Figure 1b). The core was subsampled at a 0.5–1 cm interval, and the sediment samples were subsequently freeze-dried. To compare the lake deposits with possible sediment sources, six sediment samples from the creeks and hills in the catchment were also collected. The optical lithological inspection of the core CFL-3 highlighted two distinct white clay layers at

135.3–140.7 and 168.3–171.7 cm core depth which were regarded as event layers and not included in any further analysis. The core top 0–19.3 cm was also not considered for further analysis due to established impact of human activity in the vicinity of the lake over the last 100 years according to historical records (Lin, 1996).

The daily water level fluctuations of Cueifong Lake were also recorded with a water level logger (PS 9800 (1), Instrumentation Northwest Inc., WA, USA) installed in a stationary monitoring station from September 2017 to December 2019, with missing data from 10 January 2018 to 15 May 2018 due to equipment failure.

### Age model

The CFL-3 sediment core chronology was established with a combination of  $^{210}\text{Pb}$  dating in the top 41.5 cm and  $^{14}\text{C}$  dating from 31 to 185 cm depth. For the  $^{210}\text{Pb}$  dating, sediment samples were taken at 4-cm intervals and pretreated following the method of Huh et al. (1987). Dried sediment samples were heated to 105°C and 550°C to remove water and organic material. After adding  $^{209}\text{Po}$  (40.04 dpm/g) as a tracer;  $\text{HNO}_3$  (65%),  $\text{HF}$  (40%) and  $\text{HClO}_4$  (70%) were added in sequence to remove carbonates, silicates and organic matter, respectively. Samples were plated onto silver plates in  $\text{HCl}$  (1.5 N). The  $^{210}\text{Pb}$  measurements were made with an  $\alpha$ -spectrometer (ORTEC, 576A) at the Institute of Oceanography, National Taiwan University. The sedimentation rate calculation adopted the advection-diffusion model of Huh and Su (1999) with two assumptions: (i) the flux of sediment

and  $^{210}\text{Pb}$  concentration were constant and (ii) mixing processes were disregarded. The results provide an apparent (maximum) sedimentation rate.

For the Accelerator Mass Spectrometry (AMS)  $^{14}\text{C}$  dating, fourteen samples of wood fragments or leaf debris were selected from the depth interval 50–185 cm. The samples were pretreated with an acid-base-acid (ABA) sequence to remove carbonates and mobile organic acids, as described by Brock et al. (2010). The ABA pretreatment and AMS radiocarbon dating were performed in the NTUAMS Lab, Department of Geosciences, National Taiwan University. The ages were converted into calendar years before present (0 BP=1950 CE) with the CALIB 7.10 program with the IntCal13 calibration curve (Reimer et al., 2013). Lastly, all available age tie points were used to generate a Bayesian age model for the CFL-3 core using the Bacon 2.2 R package (Blaauw and Christen, 2011).

### Grain size analysis

Grain-size changes in sediments can reflect changes in source materials (e.g. Li et al., 2017; Vandenberghe, 2013), sediment transport processes (e.g. Dietze et al., 2014; Meyer et al., 2020), deposition depth in the basin (e.g. Menking, 1997; Xiao et al., 2008, 2015), precipitation amount and river discharge (e.g. Meyer et al., 2020; Zhou et al., 2012). Core samples taken with 4-cm resolution, and all sediment trap samples, were analysed for their grain-size distributions. The sample preparation for grain-size analysis followed the United States Geological Survey (USGS) procedures as outlined by Poppe and Polloni (2000). In summary, 0.5 g of freeze-dried sediment was treated with  $\text{H}_2\text{O}_2$  (15%) and HCl (10%) for the removal of organic material and carbonate, respectively. Prior to measurement,  $\text{Na}(\text{PO}_3)_6$  (10%) was added to impede sediment coagulation. The sediment samples were measured five times for 30 s with a Beckman Coulter LS 13 320 Laser diffraction particle size analyser at the Institute of Oceanography, National Taiwan University. The detection range of the analyser is between 0.4–2000  $\mu\text{m}$ . The data of the five measurements were averaged using LS 13 320 XR ADAPT Software. The bulk grain size indices, such as mean grain size and sorting, were calculated based on the formula of Folk and Ward (1957).

Previous studies have used different grain-size based proxies to assess the environmental variations recorded in loess, peat bogs, lake sediments and marine sediments, considering mean grain size (e.g. Kang et al., 2018; Tu et al., 2017; Yang et al., 2015), standard deviation (e.g. Boulay et al., 2003; Li et al., 2017), ratios between two grain-size ranges (e.g. Ding et al., 1995; Liu et al., 2016), Weibull-distributions (e.g. Xiao et al., 2008), principal components of grain size (e.g. Hu et al., 2012) and end member modelling analysis (EMMA) (e.g. Dietze et al., 2012, 2014; Weltje et al., 2015). From the methods above, EMMA has the advantage that it is able to decompose grain-size distributions into quantified subpopulations that can be attributed to distinct sediment sources or processes (Dietze et al., 2012, 2014). Furthermore, this method does not require any beforehand, case-specific assumptions regarding the involved sedimentary processes (Dietze et al., 2014; Prins et al., 2007). End-member (EM) modelling of the grain-size distribution results of the sediment traps and core sediment samples were applied utilizing the EMMAgeo package v 0.9.7 in R 4.0.3 (Dietze and Dietze, 2019). The EM method reduces grain-size distributions of samples into significant subpopulations, that is end members, which represent idealized characteristics of grain-size composition (Dietze et al., 2012). The robust EMMA function in the R package produces several end members together with each EM's uncertainty concerning both grain size composition of each EM (loadings) and relative EM proportion of the samples (scores). We performed end-member analysis on the combination of both core and trap sediments to increase the number of samples for a robust

statistical analysis. The similarity of the resultant end members in comparison to independent core and trap sample EMMA results supports this approach.

### Principal component analysis (PCA)

In order to visualize the overall EAWM trend derived from available EAWM proxy records (Table 2; locations are shown in Figure 1a) in a dimensionally reduced space, we applied PCA. The PCA was performed using the program PAST (Hammer et al., 2001). Prior to the PCA all data sets were resampled at 100 year levels, converted into a log-ratio and scaled using z-score (mean and standard deviation) normalization. Afterwards the data structure was visually checked via histograms. The resulting data has a quasi-Gaussian probability constituting a prerequisite for the application of a PCA.

### Lipid biomarker analysis

In this study, we utilized *n*-alkanes as a lipid biomarker proxy for paleoclimate reconstruction. The *n*-alkane chain length distributions have been used extensively to discriminate between source organisms (Bingham et al., 2010; Nichols et al., 2006; Zhou et al., 2010). Well-established *n*-alkanes chain length ratios, such as the relative proportion of mid-chain to long-chain *n*-alkane homologues ( $P_{\text{aq}}$ ) as an indicator for input of submerged vascular macrophytes is also applied to the sedimentary core from Cueifong Lake.

Following the pretreatment procedure of Yamoah et al. (2016), sediment core samples were sub-sampled at ~10 cm intervals and freeze-dried. Samples were ground into fine powder before three successive extractions using a mixture of dichloromethane and methanol (DCM–MeOH, 9:1, v/v) and a sonicator to obtain a combined total lipid extract (TLE). The aliphatic compounds of the TLE were analysed with a gas chromatograph connected to a flame ionization detector (GC-FID, Agilent 7890) in the Department of Oceanography, National Sun Yat-Sen University. A dimethylpolysiloxane capillary (60 m length, 250  $\mu\text{m}$  bore and 0.25  $\mu\text{m}$  film thickness) was used in this analysis. The temperature settings follow Yamamoto et al. (2000). GC was set to 330°C with He at 31.25 psi, 1.6 ml/min as a carrier gas. The external standard (DRH-008S-R1) contained a mixture of *n*-alkane numbers from *n*-C<sub>8</sub> to *n*-C<sub>30</sub> with known concentrations and was used to establish a calibration curve. The individual *n*-alkane abundances identified from the sediment record was used to develop a  $P_{\text{aq}}$  index (Ficken et al., 2000), a proxy for the relative abundance of aquatic plants relative to terrestrial plants, using the formula below:

$$P_{\text{aq}} = \frac{C_{23} + C_{25}}{C_{23} + C_{25} + C_{29} + C_{31}}$$

## Results

### Chronology of sediment core CFL-3

As noted above, the age model of the core CFL-3 was constructed by combining  $^{210}\text{Pb}$  and  $^{14}\text{C}$  dating. The transition between the two age models occurs at a depth of 27.5 cm. The  $^{210}\text{Pb}$  activity at the core top is 35.96 dpm/g, and this value decreases exponentially until a depth of 27.5 cm, indicating that the age at this depth is ~150 years (Figure 2a). The  $^{210}\text{Pb}$  value remains relatively stable below 27.5 cm depth, and allows for the determination of supported  $^{210}\text{Pb}$ , which is  $1.59 \pm 0.61$  dpm/g, based on the averaged value of the three lowest measurement points. The average sedimentation rate for the uppermost 27.5 cm is 0.18 cm/year.

The radiocarbon dating results indicate that the base of CFL-3 reaches 2860 cal. BP (Table 1). Two outlying dating results

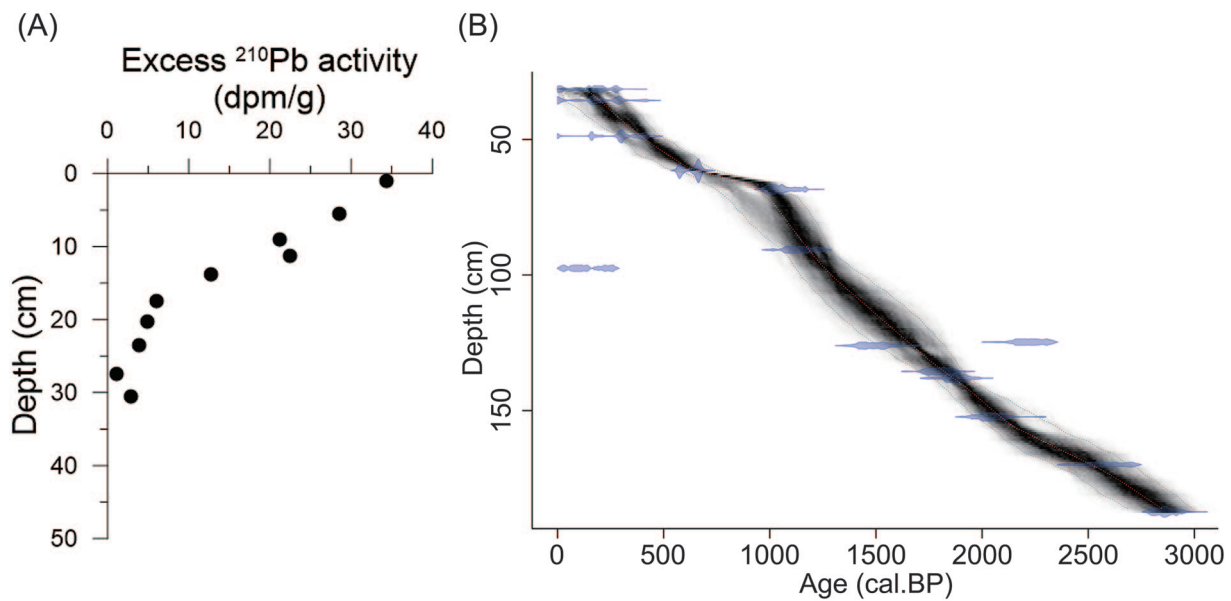


**Figure 2.** (A) Excess  $^{210}\text{Pb}$  activity in the top 41.5 cm of CFL-3. (B) Bayesian age model of core CFL-3. Radiocarbon dates (AMS  $^{14}\text{C}$ ) are calibrated with  $2\sigma$  uncertainties. Grey shades represent the model's 95% probability intervals.

**Table 1.** Radiocarbon dates and the corresponding calibrated ages of the core CFL-3. Uncalibrated ages with  $1\sigma$  uncertainty and calibrated ages with  $2\sigma$  uncertainties.

Sample ID	Depth (cm)	Uncalibrated $^{14}\text{C}$ age (year BP)	Calibrated age (calendar year BP)
CFL-3-0-100-38	31.5	$175 \pm 38$	180 (0–298)
CFL-3-0-100-42	35.6	$216 \pm 46$	195 (0–427)
CFL-3-0-100-58	48.7	$258 \pm 36$	305 (0–452)
CFL-3-0-100-76	61.5	$688 \pm 35$	655 (560–686)
CFL-3-0-100-84	68.4	$1138 \pm 33$	1040 (967–1173)
CFL-3-0-100-108	90.7	$1217 \pm 41$	1145 (1013–1267)
CFL-3-85-185-11	97.52	$124 \pm 31$	125 (10–273)
CFL-3-85-185-42	124.72	$2217 \pm 48$	2230 (2124–2340)
CFL-3-85-185-44	126.07	$1608 \pm 53$	1495 (1379–1616)
CFL-3-85-185-58	135.57	$1866 \pm 36$	1805 (1715–1879)
CFL-3-85-185-63	138.07	$1931 \pm 38$	1880 (1743–1989)
CFL-3-85-185-82	152.32	$2070 \pm 39$	2040 (1935–2142)
CFL-3-85-185-102	169.97	$2494 \pm 40$	2585 (2382–2740)
CFL-3-85-185-126	187.32	$2767 \pm 34$	2860 (2784–2946)

**Table 2.** The list of published proxy records interpreted to represent EAWM variability that have been used for establishing the EAWM index.

Core ID	Longitude	Latitude	Sample type	Proxy	Water depth (m)	Number of $^{14}\text{C}$ datings in 3000 years	Sediment length in 3000 years (m)	References
YS01	122.49E	35.52N	Marine sediment	Mean grain size ( $\mu\text{m}$ )	58.5	5	4.5	Wang (2014)
B24	112.75E	21.5N	Marine sediment	Mean grain size of sensitive proportion ( $\mu\text{m}$ )	22.5	3*	1.4	Ge et al. (2017)
Huguang Maar Lake (HGM)	110.28E	21.15N	Lake sediment	Diatom abundance ratio (AG/CS, <i>A. granulata</i> / <i>C. stelligera</i> )	20	4*	4.1	Wang et al. (2012a)
Huangyanghe B2	102.6E 125.75E	37.42N 31.75N	Eolian sediment Marine sediment	TOC (%) Content of grain size ranges between 10.5 and 65 $\mu\text{m}$ (%)	– 64	1* 4	0.53 4	Li and Morrill (2014) Xiang et al. (2006)
FJ04	125.81E	31.68N	Marine sediment	Mean grain size ( $\mu\text{m}$ )	67	3	1.67	Sun et al. (2008)
TFL-1	121.6E	24.67N	Lake sediment	PCAI (represent for precipitation)	5	7	1.68	Wang et al. (2015)

\*The bottom dating is outside of the range of 3000 years, but still included in this compilation since that point also offers additional constrain to age models used.

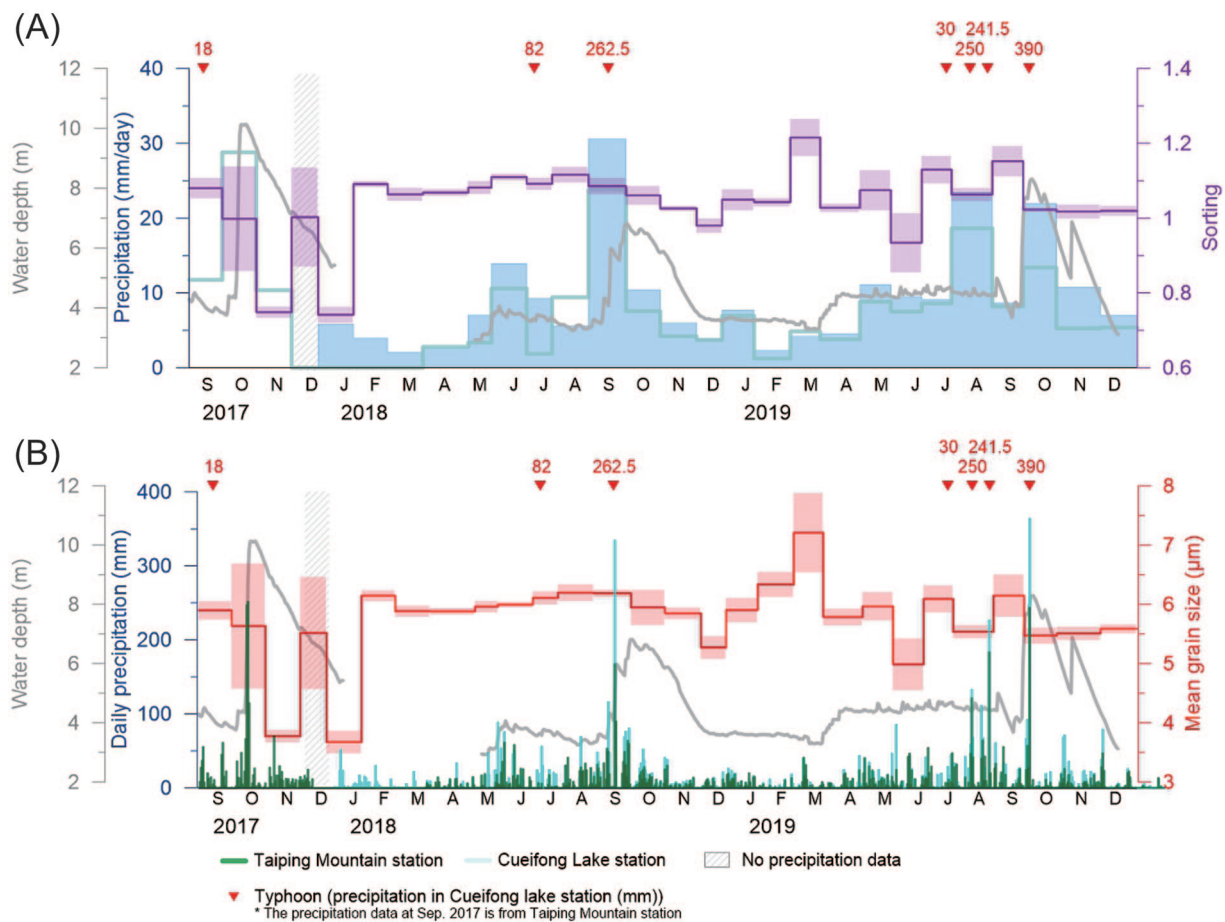


**Figure 3.** Variations in (A) sorting and (B) mean grain size of monthly collected sediments in Cueifong Lake from September 2017 to December 2019. The grey line represents lake level, shaded bars represent the standard deviation of (A) sorting and (B) mean grain size from the four tubes in the same month. The precipitation data in (A) shows the daily average precipitation during the sample collection period (i.e. about 1 month), while the precipitation data in (B) shows the daily precipitation during the observed periods.

(CFL-3-85-185-11 and CFL-3-85-185-42) do not fit the Bayesian age model (Figure 2b) and were excluded. The younger age of CFL-3-85-185-11 (leaf debris) at depth 97.5 cm is likely caused by contamination during coring or sampling, while the older age of CFL-3-85-185-42 (wood fragment) at depth 124.7 cm might be caused by contamination, or the sample had resided in the catchment for a longer period of time before being flushed into the lake. The modelled ages show a long-term sedimentation rate of  $\sim 0.058$  cm/year. Two periods of enhanced sedimentation rate of  $\sim 0.21$  cm/year and  $\sim 0.13$  cm/year fall around 1145–1040 cal. BP (90.7–68.4 cm depth) and about 310–180 cal. BP (48.7–31.5 cm depth), respectively. Between the two fast sedimentation rate periods, a period of low sedimentation rate ( $\sim 0.018$  cm/year) is found during 1040–655 cal. BP (61.5–68.4 cm depth) (Figure 2b).

#### Precipitation variability and lake level change

The monthly average precipitation at Cueifong Lake shows that the average precipitation from September 2017 to December 2019 is 315 mm/month, with the highest monthly precipitation (933 mm) in September 2018 and the lowest (66 mm) in February 2019. Several months with high precipitation (July 2018, September 2018, July–September 2019) are caused by typhoon events (typhoon-induced precipitation/total precipitation: July 2018: 86/213.5 mm, September 2018: 336.5/933 mm, July 2019: 45/233 mm, August 2019: 503/876 mm, September 2019: 429/764 mm). If the precipitation brought by typhoon events is excluded, the month with highest precipitation is October 2017 (898.5 mm) (Figure 3). The daily precipitation records also show the precipitation characteristics in Cueifong Lake between

spring-summer (March–September) and autumn-winter (October–February). In the spring-summer period, intense rain events are more likely (average monthly precipitation = 357 mm, days with daily precipitation  $> 50$  mm = 1.8 days/month), compared with autumn-winter precipitation (average monthly precipitation = 263 mm, days with daily precipitation  $> 50$  mm = 0.8 days/month).

The lake level in Cueifong Lake between 2017 and 2019 shows an annual cycle with low lake level in summer and high level in autumn-winter. The lake sustained a high level from October 2017 to January 2018, which corresponded with the winter rainy season. High lake levels also appeared after typhoon events (September 2019), although subsided relatively quickly during the month following the typhoon (Figure 3) due to the high evaporation during summer and early autumn.

#### Grain size variation in sediment trap material and core CFL-3

The combined grain-size analysis from monthly collected trap sediments and the sediment core from Cueifong Lake (September 2017 to December 2019) yields two significant grain-size end-members with an explained variance of 0.46 (Figure 4a). In general, EM 1 predominantly consists of fine to middle-silt with a main mode grain-size of  $\sim 2.9$   $\mu$ m (min–max: 1.0–6.8  $\mu$ m). EM 2 shows a dominant composition of clay to fine-silt with a main size fraction of  $\sim 10.8$   $\mu$ m (min–max: 6.2–33.0  $\mu$ m).

In detail, the monthly sediment trap samples from September 2017 to December 2019 are predominately composed of clay and silt with mean contributions of  $\sim 33.8\%$  (min–max: 22.9–61.1%)

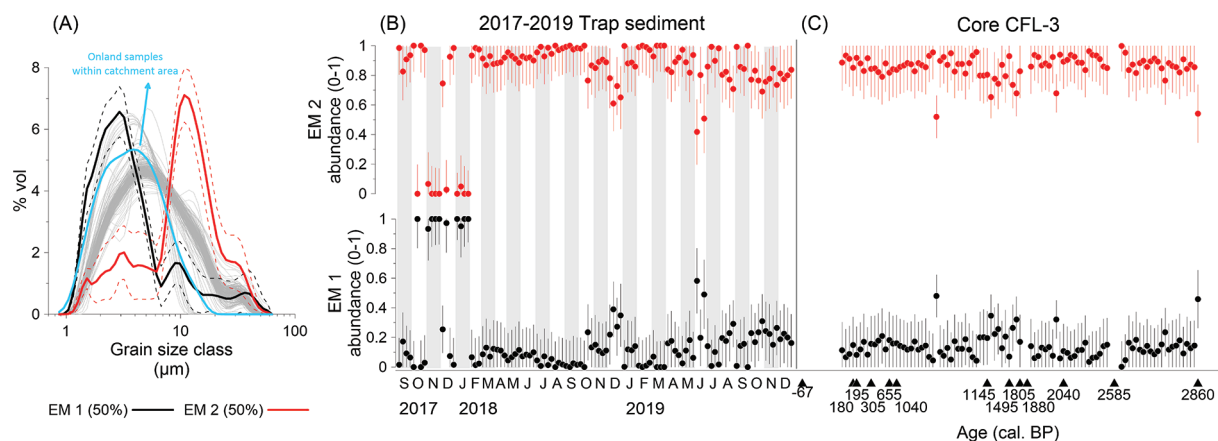


**Figure 4.** (A) The measured grain-size distributions (grey thin lines) and the mean loadings of modelled robust EM proportions (thick lines) of the combined dataset of trap and core sediment in Cueifong Lake. Dash lines indicate one-sigma standard deviation of the EMs. Light blue line shows the average grain-size distribution of clay samples taken from the surrounding catchment. (B) Mean end-member scores in each sample of the sediment trap samples in Cueifong Lake, with 1 standard deviation noted. (C) Mean end-member scores in each sample of core CFL-3, with 1 standard deviation noted.

and ~66.2% (min–max: 38.9–77.1%), respectively. Based on the relative silt contribution, two groups can be identified: (i) samples taken from November 2017 to January 2018 (winter season with strong EAWM impact), characterized by lower silt proportion (mean silt content = 51.3%); and (ii) samples taken from September 2017 to October 2017, and from February 2018 to December 2019, with higher silt proportions (mean silt content = 68.0%). The grain size characteristics of these two groups are distinctly different in the result of a cluster analysis run with the Past 3 software (see the Supplemental Material). The sorting in all trap sediments ranges between 0.72–1.27, with relatively well-sorted values (0.74–1.00) during strong EAWM-affected winters, and poorly sorted values (0.76–1.27) during the remaining seasons (Figure 3a). The distinctively varying grain-size signature of the sediment trap samples between winter and the other seasons is further mimicked by the mean grain-size values. The mean grain-size values of the sediment trap samples range between 3.43–7.87  $\mu\text{m}$ , with an overall mean value of  $5.73 \pm 0.77 \mu\text{m}$ . The mean grain size range in winter months is 3.42–6.18  $\mu\text{m}$ , while in other seasons it is 3.82–7.87  $\mu\text{m}$  (Figure 3b).

In the CFL-3 core, the sediment profile is also dominated by clay and silt, with mean contributions of ~31.1% (29.0–43.6%) and ~68.9% (56.4–71.0%), respectively. The mean grain-size value in this core ranges 4.20–6.62  $\mu\text{m}$  (average of  $5.79 \pm 0.34 \mu\text{m}$ ), while the sorting range is 0.77–1.21. Both mean grain size and sorting values are characterized by a relatively stable signal from 2860 cal. BP to recent, with five distinct decreases during 2860–2845 cal. BP, 2540–2425 cal. BP, 1140–1120 cal. BP, 33–17 BP and 1987–2017 CE (Figure 5).

#### Lipid biomarker variation in core CFL-3

The  $P_{\text{aq}}$  index in the sediment core CFL-3 ranges between 0.07 and 0.29. The  $P_{\text{aq}}$  index shows higher aquatic macrophytes dominant signal during two periods (2730–2560 and 1810–1550 cal. BP). From 1240 cal. BP to 1970 CE (core top), the  $P_{\text{aq}}$  index shows a low average value. The lowest value, at 0.07, falls around 520 cal. BP (Figure 5).

## Discussion

### Sediment grain-size distribution in Cueifong Lake and its environmental implications

Two end members were extracted from both trap and core sediment results, EM 1 (fine grain proportion, ~2.9  $\mu\text{m}$ ) is interpreted as fine clay particles from the catchment, as it matches the

grain-size distribution of clay samples taken from the surrounding hills of Cueifong Lake (Figure 4a). We regard EM 2 (coarser proportion, ~10.8  $\mu\text{m}$ ) as fluvial reworking suspension, based on the similar grain size range as previous studies in other lakes shows (Liu et al., 2016; Vandenberghe, 2013).

We find that the relative contribution of the two end-members to grain-size are seasonally dependent at Cueifong Lake (Figure 4b). EM 1 consisting of clay-size particles occurs most persistently during autumn to winter months (October–January) throughout the studied time interval. In contrast, EM 2 (fine to middle silt fraction) dominates during the summer month (June–August). This seasonal change in sediment supply to the lake centre could represent changes in the energy regime of the sediment transport towards the lake. Intense precipitation over the catchment area during the summer months increases surface runoff that mobilizes coarser particles for transport (Hsu et al., 2013; Kiani-Harchegani et al., 2019). In contrast, the less intense but persistent winter precipitation would not facilitate an increased transport of coarse detritus towards the lake centre.

In addition to transport energies, the varying transport distances, controlled by the strongly seasonally varying lake level, likely influences the grain size of the deposited sediment. The highest lake levels in Cueifong Lake generally coincide with the winter season (Figure 3). Albeit winter precipitation is less intense than during the summer months, the lower air temperatures reduce evaporation rates which in turn leads to high lake levels during winter (Chen and Chen, 2003; Chen and Huang, 1999; Yen and Chen, 2000). High lake levels in turn increase the distance between shoreline and lake centre, and thus trap coarser sediments on the lake margins (Menking, 1997; Xiao et al., 2008, 2015). The high precipitation amount during summer (July–September 2017) is counteracted by the increased evaporation due to high surface summer air temperatures (Figure 1c), which leads to a lowering of the lake level during the summer months relative to the winter months (Figure 3). The relationship between lake level and the abundance of coarser/finer sediments in the lake centre is also mimicked by a significant difference in sediment sorting between the winter and summer months (Figure 3a). As transport distances increase with rising lake levels, sediments tend to be better sorted (Folk and Ward, 1957; Gao et al., 1994), which corresponds with the better-sorted sediments in November 2017–January 2018 (Figure 3a).

Interestingly, EM 2 (coarse grains) in our 2-year observation time series was always dominant during summer months but varied greatly during the three studied winter periods of 2017/2018, 2018/2019 and 2019/2020. Whereas the winter of 2017 is

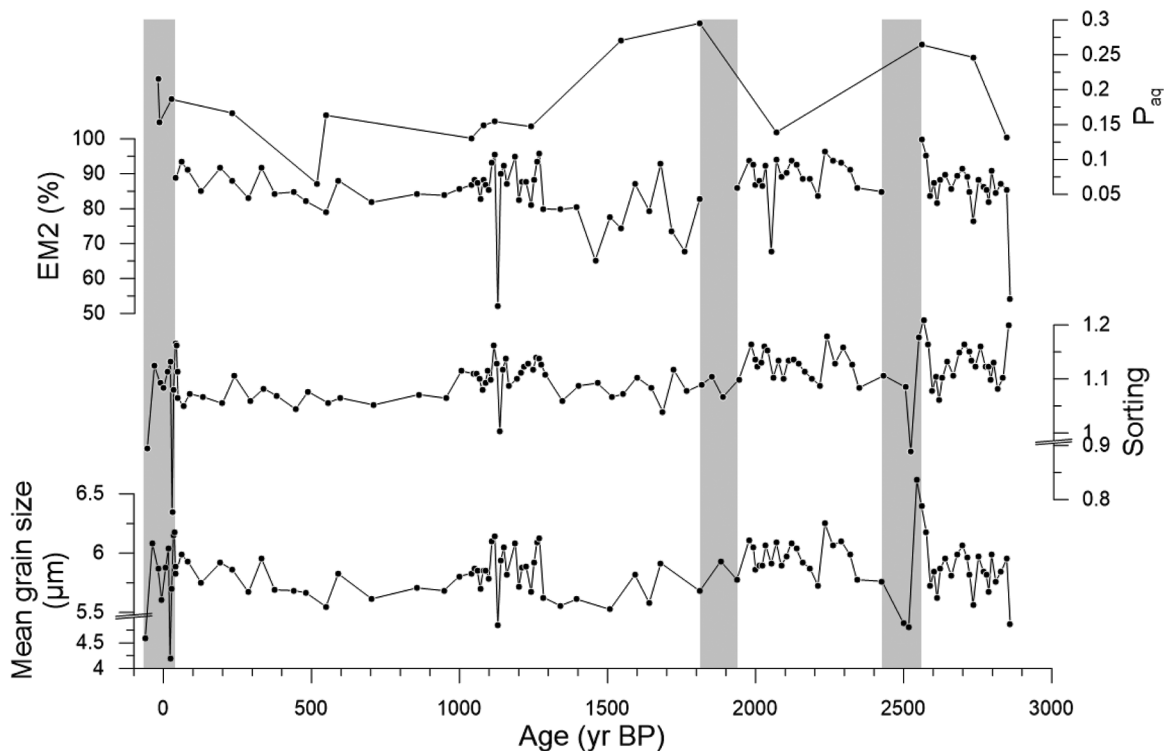


**Figure 5.** Downcore variations of sorting and mean grain size of sediment core CFL-3. Grey bars denote periods with decreases of both sorting and mean grain-size values.

dominated by almost exclusively fine sediments the sediments representing winter 2018/2019 and 2019/2020 show a marked increase of clastic material (Figure 3b). We argue that the increase of EM 2 is inversely related to the strength of the EAWM which drives the winter precipitation intensity and amounts at Cueifong Lake. Observational data shows that the overall EAWM strength increased during the winter of 2017/2018 relative to the weaker EAWM years of 2018/2019 and 2019/2020. The average surface air pressure from November to February shows that the Siberian High had a positive anomaly (i.e. stronger than average) during 2017/2018 winter. This is highlighted by prevailing northeast winds in northeastern Taiwan during the winter of 2017/2018 whereas south and east wind persisted during the winters of 2018/2019 and 2019/2020 (see the Supplemental figure). The EAWM strength variation between the three observed winters also clearly affected lake level, with a stronger EAWM during winter (2017/2018) resulting in relatively abundant precipitation which led to higher lake levels (Figure 3). As a consequence, the sediments of winter 2017/2018 are overall finer than compared to winter 2018/2019 and 2019/2020 (Figure 4b). Hence, we argue that EM 2 is a robust and sensitive proxy of lake level and transport energy and thus of EAWM strength.

A higher EM 2 content is evident in June 2019 although it was a summer month (Figure 4b), and there was neither a significant lake level change nor an intense precipitation event (Figure 3b). However, only three out of the four tubes were available for the June 2019 samples, and neither sample weight nor grain size distribution patterns were identical in between the three tubes. Thus we regard the inconsistency as disturbance during field sampling, also reflected by the larger error bar in the monthly averaged data (Figure 3).

#### *East Asian winter monsoon (EAWM) variability in the last 3000 years*

Our findings from the sediment trap at Cueifong Lake clearly show that changes in the grain-size distribution of deposited

sediments are directly linked to seasonal rainfall and lake level variability, with the most pronounced grain-size changes occurring in winter. In turn, winter precipitation amount is predominantly controlled by the strength of the EAWM (Chen and Chen, 2003; Chen and Huang, 1999; Yen and Chen, 2000) (see section 2.2). Thus, we argue that grain-size changes in Cueifong Lake sediments might also prove to be a useful tracer for EAWM variability on longer time scales.

In fact, the combined grain-size end-member modelling of both, monthly collected trap sediment samples and the sediment core, highlight strong similarities in their grain-size distributions. In both cases, EM 2 comprises predominantly silt-sized particles while EM 1 is associated with finer, mostly clay-sized particles. Thus, based on the established modern linkage between EM 2 and EAWM variability we propose that the EM 2 record in sediment core CFL-3 can be interpreted as representative of EAWM strength throughout the 3000 years. In this scenario, smaller contributions of EM 2 to the sedimentary regime at Cueifong Lake would reflect stronger EAWM and vice versa (Figure 5).

To further test the robustness of EM 2 as a proxy of Holocene EAWM variability, we compared it with  $P_{aq}$ , a biomarker index that shows the proportion between aquatic plants relative to terrestrial plants (Figure 5) (Ficken et al., 2000). On an annual basis, an increase in aquatic macrophytes is tightly coupled to a higher availability of dissolved nutrients, and vice versa (Tsai et al., 2011). Hence, higher lake levels of Cueifong Lake during strong EAWM phases lead to dilution of dissolved nutrients and a decrease in aquatic productivity. In contrast, a weaker EAWM leads to lower lake levels and increase in dissolved nutrients content that will support aquatic productivity (Tsai et al., 2016).  $P_{aq}$  and EM 2 show a positive relationship, which supports that both proxies independently reflect an EAWM signal, with an increase in  $P_{aq}$  and in EM 2 during weak EAWM phases.

Based on the variability of EM 2 and  $P_{aq}$ , we infer a long-term trend of increasing EAWM strength from the late-Holocene to the recent, superimposed by two distinct phases of strongly weakened EAWM between 2250–1600 and 1300–900 cal. BP (Figure 6c). In



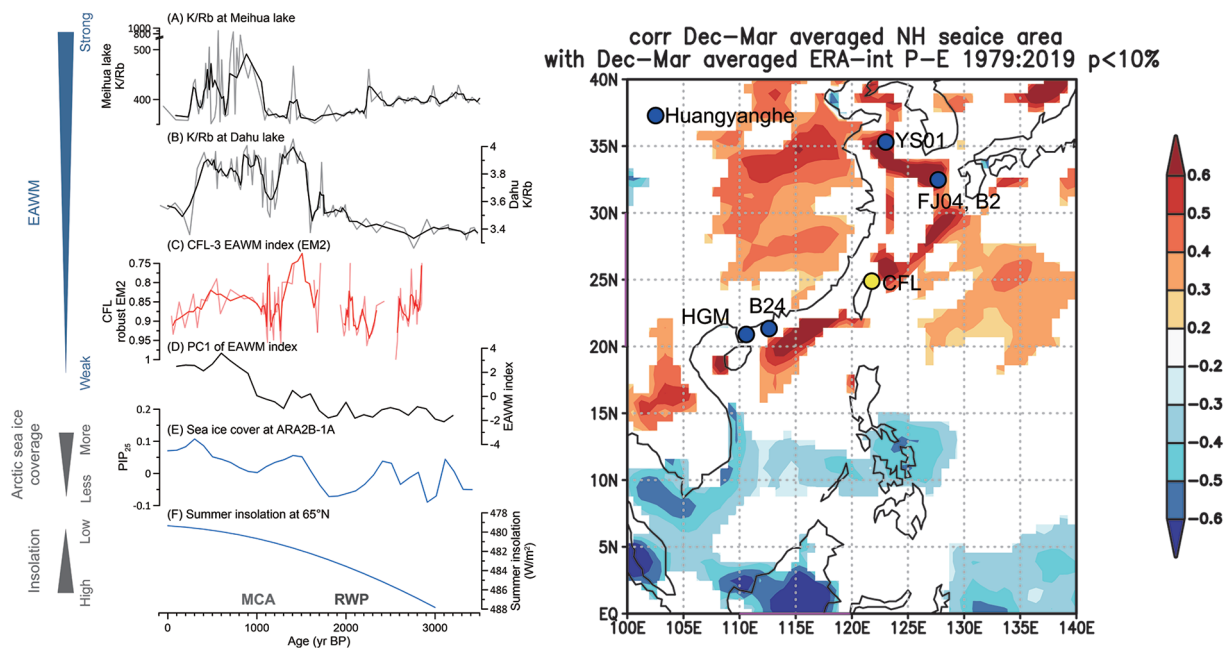


**Figure 6.** Comparison between (A) K/Rb ratio in Meihua lake (Chen et al., 2012), grey line shows the original data and black line is the three-point running mean. (B) K/Rb in Dahu lake (Chen et al., 2012), grey line shows the original data and black line is the three-point running mean. (C) The proportion of EM 2 of core CFL-3 (this study), light red line shows the original data and red line is the three-point running mean. (D) EAWM index based on PC 1 of regional EAWM records (Ge et al., 2017; Li and Morrill, 2014; Sun et al., 2008; Wang, 2014; Wang et al., 2012a, 2015; Xiang et al., 2006). (E) PIP<sub>25</sub> biomarker record of Arctic sea-ice coverage (Stein et al., 2017) and (F) Northern hemisphere summer insolation. The two grey bars represent the Roman Warm Period (RWP) (Wang et al., 2012b) and Medieval Climate Anomaly (MCA) (Mann et al., 2009). (G) Correlation coefficient ( $p < 0.1$ ) between December to March, Northern Hemisphere (NH) sea-ice extent and surface humidity (potential evaporation) derived from the global atmospheric reanalysis ERA-Interim for the time period between 1979 and 2019, red = positive correlation coefficient; blue = negative correlation coefficient. Blue dots indicate the geographical position of other EAWM records referenced in the main text (see also Table 2). Yellow dot indicates the study area. Analysis and graphic visualization were conducted using Climate Explorer (<https://climexp.knmi.nl/>).

this scenario, stronger EAWM corresponds to a decrease in both coarser detrital input and aquatic productivity. In contrast, the sediment coarsening and increased production of aquatic macrophytes between 2250–1600 and 1300–900 cal. BP signal a distinct decrease in EAWM strength. The gradual EAWM increase recorded in core CFL-3 is in accord with the gradual cooling trend and increased precipitation reconstructed by pollen in Cueifong Lake (Wang et al., 2015). The increase in EAWM is also found in the low-land lake record of the Ilan plain, in close proximity to our study site (Figure 6a–c) (Chen et al., 2012; Lin, 2004). The suggested intense chemical weathering episodes between 1650–1250 and 1000–300 cal. BP at Dahu Lake, interpreted as increased EAWM, fit well with phases of strong EAWM based on our results (Figure 6b) (Chen et al., 2012). For Meihua Lake, also located in the same geographical region as Dahu Lake, the EAWM phases have been reconstructed from the K/Rb ratio and appear to lag behind the increased EAWM phases inferred from Cueifong Lake (Figure 6a) (Chen et al., 2012). This could potentially be attributed to age model uncertainties between our chronology and Dahu Lake. However, the K/Rb signal of Meihua Lake might be distorted by enhanced riverine sediment supply as similar timed river-aggradation periods have been postulated (Huang et al., 2019).

To disentangle potential local to regional EAWM variability we compared our EM 2 record from Cueifong Lake to seven established EAWM reconstructions from the East Asian realm. These records combine marine and terrestrial sites from a wider region. Interestingly, the long-term increase in EAWM strength during the late-Holocene that we find in our EM 2 record at Cueifong Lake can also be clearly identified in six out of seven EAWM reconstructions (see the Supplemental data). This implies that the long-term increase of EAWM is an intrinsic and supra-regional signal. In contrast, the two pronounced phases of EAWM

weakening depicted in the EM 2 of Cueifong Lake are only mirrored by a similar variability in the TOC (%) record at Huan-yanghe located in central China. The centennial scale divergences of the different EAWM reconstructions relative to Cueifong Lake might be attributable to (i) the temporal resolution of the applied proxy records, (ii) differences in chronological accuracy, (iii) the geographical position of the sites and (iv) the sensitivity of the proxies utilized at each site.

Assuming the dating uncertainties are limited, we performed a principal component analysis (PCA; see section 3.4) of these seven well-established EAWM indices to allow a comparison between records showing the long-term evolution of the EAWM during the late-Holocene. We argue that PC 1, which explains 55% of the total variance, captures the supra-regional EAWM variability during the last 3000 years (Figure 6d). The comparison between EM 2 in core CFL-3 and PC 1, hereafter referred to as the EAWM stack, shows a similar long-term increase in EAWM strength during the late-Holocene (Figure 6c and d). This close relationship supports the robustness of EM 2 as a tracer of past EAWM variability.

Despite the overall close match between EM 2 and the EAWM stack, the two distinct phases of pronounced EAWM decline recorded in EM 2 (1260–1040 and 2290–1880 year BP), as well as in the Dahu and Meihua Lake records (Chen et al., 2012; Lin, 2004), are not mimicked by the EAWM stack (Figure 6c and d). This mismatch could be explained when considering the construction of the EAWM stack. Prior to the PCA, all data sets were resampled at the lowest resolution of all data sets used, which causes a smoothing of the individual data sets. This leads to a loss of signal variability that could be the cause of the signal mismatch between the EM 2 of CFL-3 and the EAWM stack. On the other hand, it could also be argued that EM 2 is not linearly related to EAWM variability, and that potential non-linearity could impart

exaggerated amplitude changes in the grain size regime at Cueifong Lake. The robustness of the climate features we have identified at Cueifong Lake is supported by the occurrence of similar timed wet and dry phases in other paleoclimatic records from Northern and Central Taiwan (Liew et al., 2014).

### Teleconnection between EAWM and Arctic sea ice in the late-Holocene

The long-term increase of EAWM strength during the last ~3000 years has been attributed to the orbital-driven decrease of Northern Hemisphere summer insolation (Figure 6c and f) (Hays et al., 1976; Kang et al., 2018; Sagawa et al., 2014). Decreased summer insolation caused hemisphere-wide cooling, particularly in the mid- and high-latitudes, which is evident in documented glacial advances in Europe, Russia and North America (Solomina et al., 2015), and also in increased western Arctic sea-ice coverage in the late-Holocene (Fahl and Stein, 2012; Hörner et al., 2016; Stein et al., 2017) (Figure 6e). On interannual time scales, sea-ice variability in the western Arctic Ocean is directly linked to EAWM strength (Chen et al., 2014). An increase of sea-ice coverage in the western Arctic Ocean leads to enhanced albedo, together with a significant strengthening of the Siberian High and a deepening of the East Asian trough. This process induces cooling in mid-latitude Asia and strengthens the EAWM, and vice versa for low sea-ice cover conditions (Chen et al., 2014; Wu et al., 2006; Zhang et al., 2015). The close relationship between Arctic sea-ice coverage and EAWM strength in the Holocene is also manifested on millennial time scales (Huang, 2011).

Interestingly, the two pronounced episodes of EAWM decline captured by EM 2 at Cueifong Lake align with phases of high latitude climate change associated with the Roman Warm Period (RWP, 2500–1600 BP) (Wang et al., 2012b) and Medieval Climate Anomaly (MCA, 1050–650 BP) (Mann et al., 2009), respectively (Figure 6c). Notably, during the RWP and MCA, sea-ice coverage decreases were found in the Arctic (Kinnard et al., 2011; Kolling et al., 2017), coinciding with weak EAWM phases recorded in core CFL-3 (Figure 6c). Given the documented link between increased Arctic sea-ice and strengthened EAWM (Chen et al., 2014; Wu et al., 2006; Zhang et al., 2015), the two episodes of strong EAWM decline recorded by EM 2 in CFL-3 thus likely represents a robust climate signal. In this case, the lack of a similar strong expression of EAWM decline in the EAWM stack might be an imprint of the strongly varying regional sensitivity to the relationship between EAWM strength and Arctic sea-ice changes (Figure 6d and e). The high sensitivity of EM 2 from sediment core CFL-3 to hydroclimatic changes is thus a testimony to the strong positive correlation between winter precipitation changes in Northern Taiwan and Arctic sea-ice variability (Figure 6g).

Based on the documented sensitivity of northeastern Taiwan to EAWM changes, it is feasible to argue that the proposed rapid decline of Arctic sea-ice as predicted for the next decades (IPCC, 2014) will most likely trigger a decrease of EAWM strength and therefore increased winter drought in northeastern Taiwan. As winter rainfall provides an important source for yearly precipitation in northeastern Taiwan and plays an important role in the development of local agriculture (Li, 1999; Yen and Chen, 2000), a reduced EAWM strength might severely impact the socio-economic conditions in this region in the future.

### Conclusions

Based on grain-size analysis from trap sediments sampled monthly, and down-core data (CFL-3) from Cueifong Lake, northeastern Taiwan, the following conclusions can be made:

1. Trap sediments collected monthly from September 2017 to December 2019 reveal a decrease in sediment grain size that corresponds to periods of sustained high lake levels. Sustained high lake levels in Cueifong Lake occur in winter, which is the EAWM-related rainy season in northeastern Taiwan.
2. End-member analysis of sediment trap and down-core data identifies two end-members: EM 1 and EM 2. We show that the EM 2 can serve as a proxy of EAWM strength, with lower EM 2 reflecting stronger EAWM.
3. A gradual strengthening of the EAWM during the past ~3000 years was observed for northeastern Taiwan, in accord with other EAWM records. The gradual strengthening of the EAWM is apparently linked to enhanced sea-ice cover in the western Arctic Ocean, driven by a decrease of summer insolation in the late-Holocene.
4. Superimposed, centennial-scale decreases in EAWM intensity relate to concomitant decreases of Arctic sea-ice cover during the RWP and the MCA. This testimony of sensitivity between Arctic sea-ice cover loss and winter droughts in northeastern Taiwan potentially provides an important background to allow prediction and mitigation for future global climate change.

### Acknowledgements


We thank the Forestry bureau Luodong forest district office and Cueifong villa for providing access to the study area and assisting with field work. We also like to extend our appreciation to Mr. Ching-Han Huang for providing photos and historical literature about Cueifong Lake. We thank Wayne Yuan-Huai Tsai for calculating seasonal mean sea level pressure and 850-hPa wind direction as a yearly EAWM index.


### Funding


The author(s) disclosed receipt of the following financial support for the research, authorship, and/or publication of this article: This work was supported by the Ministry of Science and Technology (Taiwan) (grant numbers 109-2927-I-002-508) and the Featured Areas Research Center Program within the framework of the Higher Education Sprout Project by the Ministry of Education (MOE) of Taiwan. SKB received funding from the German Academic Exchange Service (DAAD) under grant number 57558354 as well as from an Open-Topic Post-Doc fellowship from the University of Potsdam.

### ORCID iDs

Tsai-Wen Lin  <https://orcid.org/0000-0002-2244-3705>

George Burr  <https://orcid.org/0000-0003-0068-7589>

Yuan-Pin Chang  <https://orcid.org/0000-0001-8147-7860>

Chih-Chieh Su  <https://orcid.org/0000-0002-7624-1607>

### Supplemental material

Supplemental material for this article is available online.

### References

- Bingham EM, McClymont EL, Väiliranta M et al. (2010) Conservative composition of n-alkane biomarkers in Sphagnum species: Implications for palaeoclimate reconstruction in ombrotrophic peat bogs. *Organic Geochemistry* 41(2): 214–220.
- Blaauw M and Christen JA (2011) Flexible paleoclimate age-depth models using an autoregressive gamma process. *Bayesian Analysis* 6(3): 457–474.
- Boulay S, Colin C, Trentesaux A et al. (2003) Mineralogy and sedimentology of Pleistocene sediment in the South China Sea (ODP Site 1144). *Proceedings of the Ocean Drilling Program, 184 Scientific Results* 184(211): 1–21.

- Brand S and Belloch JW (1974) Changes in the characteristics of typhoons crossing the island of Taiwan. *Monthly Weather Review* 102(10): 708–713.
- Brock F, Higham T, Ditchfield P et al. (2010) Current pretreatment methods for AMS radiocarbon dating at the Oxford radiocarbon accelerator unit (Orau). *Radiocarbon* 52(01): 103–112.
- Central Weather Bureau (2009) Statistics of climate changes in Taiwan 1897–2008. Central Weather Bureau, Ministry of Transportation and Communications.
- Chen C-S and Chen Y-L (2003) The rainfall characteristics of Taiwan. *Monthly Weather Review* 131(7): 1323–1341.
- Chen C-S and Huang J-M (1999) A numerical study of precipitation characteristics over Taiwan Island during the winter season. *Meteorology and Atmospheric Physics* 70(3–4): 167–183.
- Chen H-F, Wen S-Y, Song S-R et al. (2012) Strengthening of paleo-typhoon and autumn rainfall in Taiwan corresponding to the Southern Oscillation at late-Holocene. *Journal of Quaternary Science* 27(9): 964–972.
- Chen S-H, Wu J-T, Yang T-N et al. (2008) Late-Holocene paleoenvironmental changes in subtropical Taiwan inferred from pollen and diatoms in lake sediments. *Journal of Paleolimnology* 41(2): 315–327.
- Chen Z, Wu R and Chen W (2014) Impacts of autumn Arctic sea ice concentration changes on the East Asian winter monsoon variability. *Journal of Climate* 27(14): 5433–5450.
- Clift PD and Plumb RA (2008) *The Asian Monsoon: Causes, History and Effects*. Cambridge: Cambridge University Press.
- Cohen AS (2003) *Paleolimnology: The History and Evolution of Lake Systems*. New York, NY: Oxford University Press.
- Dadson SJ, Hovius N, Chen H et al. (2003) Links between erosion, runoff variability and seismicity in the Taiwan orogen. *Nature* 426(6967): 648.
- Dietze E and Dietze M (2019) Grain-size distribution unmixing using the R package EMMAgeo. *E&G Quaternary Science Journal* 68(1): 29–46.
- Dietze E, Hartmann K, Diekmann B et al. (2012) An end-member algorithm for deciphering modern detrital processes from lake sediments of Lake Donggi Cona, NE Tibetan Plateau, China. *Sedimentary Geology* 243–244: 169–180.
- Dietze E, Maussion F, Ahlborn M et al. (2014) Sediment transport processes across the Tibetan Plateau inferred from robust grain-size end members in lake sediments. *Climate of the Past* 10(1): 91–106.
- Ding Z, Liu T, Rutter NW et al. (1995) Ice-volume forcing of East Asian winter monsoon variations in the past 800,000 years. *Quaternary Research* 44(2): 149–159.
- Fahl K and Stein R (2012) Modern seasonal variability and deglacial/Holocene change of central Arctic Ocean sea-ice cover: New insights from biomarker proxy records. *Earth and Planetary Science Letters* 351–352: 123–133.
- Ficken KJ, Li B, Swain D et al. (2000) An n-alkane proxy for the sedimentary input of submerged/floating freshwater aquatic macrophytes. *Organic Geochemistry* 31(7–8): 745–749.
- Folk RL and Ward WC (1957) Brazos river bar: A study in the significance of grain size parameters. *Journal of Sedimentary Research* 27(1): 3–26.
- Fu C (2003) Potential impacts of human-induced land cover change on East Asia monsoon. *Global and Planetary Change* 37(3–4): 219–229.
- Gao S, Collins M, Lanckneus J et al. (1994) Grain size trends associated with net sediment transport patterns: An example from the Belgian continental shelf. *Marine Geology* 121(3–4): 171–185.
- Ge Q, Xue Z, Yao Z et al. (2017) Anti-phase relationship between the East Asian winter monsoon and summer monsoon during the Holocene? *Journal of Ocean University of China* 16(2): 175–183.
- Guo D, Gao Y, Bethke I et al. (2014) Mechanism on how the spring Arctic sea ice impacts the East Asian summer monsoon. *Theoretical and Applied Climatology* 115(1–2): 107–119.
- Hammer Ø, Harper DA and Ryan PD (2001) PAST: Paleontological statistics software package for education and data analysis. *Palaeontologia Electronica* 4(1): 9.
- Hays JD, Imbrie J and Shackleton NJ (1976) Variations in the Earth's orbit: Pacemaker of the ice ages. *Science* 194(4270): 1121–1132.
- Hörner T, Stein R, Fahl K et al. (2016) Post-glacial variability of sea ice cover, river run-off and biological production in the western Laptev Sea (Arctic Ocean) – A high-resolution biomarker study. *Quaternary Science Reviews* 143: 133–149.
- Hsu L-H, Kuo H-C and Fovell RG (2013) On the geographic asymmetry of typhoon translation speed across the mountainous island of Taiwan. *Journal of the Atmospheric Sciences* 70(4): 1006–1022.
- Hu B, Yang Z, Zhao M et al. (2012) Grain size records reveal variability of the East Asian winter monsoon since the middle Holocene in the central Yellow Sea mud area, China. *Science China Earth Sciences* 55(10): 1656–1668.
- Huang JJ (2011) *Linkage between Natural Disasters and Kiwulan Cultural Hiatus over the Last 1000 Years in the Lanyang Drainage (in Chinese)*. Taipei, Taiwan: National Taiwan University.
- Huang J-JS, Wei K-Y, Löwemark L et al. (2019) What caused the cultural hiatus in the Iron-Age Kiwulan site, northeastern Taiwan? *Quaternary International* 514: 186–194.
- Huh C-A and Su C-C (1999) Sedimentation dynamics in the East China Sea elucidated from 210Pb, 137Cs and 239,240Pu. *Marine Geology* 160(1–2): 183–196.
- Huh C-A, Zahnle DL, Small LF et al. (1987) Budgets and behaviors of uranium and thorium series isotopes in Santa Monica Basin sediments. *Geochimica et Cosmochimica Acta* 51(6): 1743–1754.
- IPCC (2014) Climate change 2014: Synthesis report. Contribution of working groups I, II and III to the fifth assessment report of the intergovernmental panel on climate change [Core writing team, RK Pachauri and LA Meyer (eds)]. Geneva, Switzerland: IPCC.
- Kang S, Wang X, Roberts HM et al. (2018) Late-Holocene anti-phase change in the East Asian summer and winter monsoons. *Quaternary Science Reviews* 188: 28–36.
- Kiani-Harchegani M, Sadeghi SH, Singh VP et al. (2019) Effect of rainfall intensity and slope on sediment particle size distribution during erosion using partial eta squared. *Catena* 176: 65–72.
- Kinnard C, Zdanowicz CM, Fisher DA et al. (2011) Reconstructed changes in Arctic sea ice over the past 1,450 years. *Nature* 479(7374): 509–512.
- Kolling HM, Stein R, Fahl K et al. (2017) Short-term variability in late-Holocene sea ice cover on the East Greenland Shelf and its driving mechanisms. *Palaeogeography, Palaeoclimatology, Palaeoecology* 485: 336–350.
- Lau K-M and Li M-T (1984) The monsoon of East Asia and its global associations—A survey. *Bulletin of the American Meteorological Society* 65(2): 114–125.
- Li L-F (1999) Meteorological impact on the rice yield in Yilan area (in Chinese). *Research Report of Hualien District* 17: 93–102.
- Li N, Chambers FM, Yang J et al. (2017) Records of East Asian monsoon activities in northeastern China since 15.6 ka, based on grain size analysis of peaty sediments in the Changbai Mountains. *Quaternary International* 447: 158–169.
- Li Y and Morrill C (2014) A Holocene East Asian winter monsoon record at the southern edge of the Gobi Desert and its

- comparison with a transient simulation. *Climate Dynamics* 45(5–6): 1219–1234.
- Liew P-M, Wu M-H, Lee C-Y et al. (2014) Recent 4000 years of climatic trends based on pollen records from lakes and a bog in Taiwan. *Quaternary International* 349: 105–112.
- Lin C-C (1996) *The Developing History of Taiping Mountain (in Chinese)*. Yilan, Taiwan: Forum art & antiques Co.
- Lin C-w and Lin w-h (1995) *Sanshin*. Taipei, Taiwan: Central Geological Survey.
- Lin H-C, Tsai J-W, Liu W-C et al. (2018) Seasonal pattern of lake mixing regime in a subtropical mountain lake, Taiwan (in Chinese). *Journal of Wetlands* 7(1): 23–41.
- Lin S-F (2004) *Environmental and Climatic Changes in Ilan Plain over the Recent 4200 Years As Revealed by Pollen Data and Their Relationship to Prehistory Colonization (in Chinese)*. Taipei, Taiwan: National Taiwan University.
- Liu X, Vandenberghe J, An Z et al. (2016) Grain size of Lake Qinghai sediments: Implications for riverine input and Holocene monsoon variability. *Palaeogeography, Palaeoclimatology, Palaeoecology* 449: 41–51.
- Mann ME, Zhang Z, Rutherford S et al. (2009) Global signatures and dynamical origins of the Little Ice Age and Medieval Climate Anomaly. *Science* 326(5957): 1256–1260.
- Mao J-J (2006) Investigation on the biological resources and habitat of Tsuei-Feng Lake (1/2) (in Chinese). Yilan, Taiwan: Research and conservation of Forestry Bureau, Taiwan.
- Menking KM (1997) Climatic signals in clay mineralogy and grain-size variations in Owens Lake core OL-92, southeast California. *Geological Society of America* 317: 25–36.
- Meyer I, Van Daele M, Tanghe N et al. (2020) Reconstructing East African monsoon variability from grain-size distributions: End-member modeling and source attribution of diatom-rich sediments from Lake Chala. *Quaternary Science Reviews* 247: 106574.
- Nichols JE, Booth RK, Jackson ST et al. (2006) Paleohydrologic reconstruction based on n-alkane distributions in ombrotrophic peat. *Organic Geochemistry* 37(11): 1505–1513.
- Poppe LJ and Polloni CF (2000) USGS east-coast sediment analysis; Procedures, database, and georeferenced displays. Reston, VA: United States Geological Survey, Coastal and Marine Geology Program.
- Prins MA, Vriend M, Nugteren G et al. (2007) Late Quaternary aeolian dust input variability on the Chinese Loess Plateau: Inferences from unmixing of loess grain-size records. *Quaternary Science Reviews* 26(1–2): 230–242.
- Reimer PJ, Bard E, Bayliss A et al. (2013) IntCal13 and Marine13 radiocarbon age calibration curves 0–50,000 years cal BP. *Radiocarbon* 55(4): 1869–1887.
- Sagawa T, Kuwae M, Tsuruoka K et al. (2014) Solar forcing of centennial-scale East Asian winter monsoon variability in the mid- to late-Holocene. *Earth and Planetary Science Letters* 395: 124–135.
- Shieh S-L, Wang S-T, Cheng M-D et al. (1998) Tropical cyclone tracks over Taiwan from 1897 to 1996 and their applications. CWB86-1M-01. Taipei, Taiwan: Atmospheric R & D center, Central Weather Bureau, Taiwan.
- Solomina ON, Bradley RS, Hodgson DA et al. (2015) Holocene glacier fluctuations. *Quaternary Science Reviews* 111: 9–34.
- Stein R, Fahl K, Schade I et al. (2017) Holocene variability in sea ice cover, primary production, and Pacific-Water inflow and climate change in the Chukchi and East Siberian Seas (Arctic Ocean). *Journal of Quaternary Science* 32(3): 362–379.
- Sun C and Yang S (2012) Persistent severe drought in southern China during winter-spring 2011: Large-scale circulation patterns and possible impacting factors. *Journal of Geophysical Research: Atmospheres* 117(D10): n/a–n/a.
- Sun X, Li G, Liu Y et al. (2008) Response of environmental sensitive grain size group in core FJ04 from mud area in the north of East China Sea to East Asian winter monsoon evolution. *Marine Geology & Quaternary Geology* 28(4): 11–17.
- Tsai J-W, Kratz TK, Hanson PC et al. (2011) Metabolic changes and the resistance and resilience of a subtropical heterotrophic lake to typhoon disturbance. *Canadian Journal of Fisheries and Aquatic Sciences* 68(5): 768–780.
- Tsai J-W, Kratz TK, Rusak JA et al. (2016) Absence of winter and spring monsoon changes water level and rapidly shifts metabolism in a subtropical lake. *Inland Waters* 6(3): 436–448.
- Tu L, Zhou X, Cheng W et al. (2017) Holocene East Asian winter monsoon changes reconstructed by sensitive grain size of sediments from Chinese coastal seas: A review. *Quaternary International* 440: 82–90.
- United Nations (2019) World population prospects 2019: Highlights (ST/ESA/SER.A/423), United Nations.
- Vandenberghe J (2013) Grain size of fine-grained windblown sediment: A powerful proxy for process identification. *Earth-Science Reviews* 121: 18–30.
- Wang B, Wu R and Fu X (2000) Pacific–East Asian teleconnection: How does ENSO affect East Asian climate? *Journal of Climate* 13(9): 1517–1536.
- Wang L (2014) Sediment record of paleoenvironment of the central mud of the South Yellow Sea and its response to the East Asian monsoon during Holocene. Ocean University of China, Qingdao.
- Wang L-C, Behling H, Kao S-J et al. (2015) Late-Holocene environment of subalpine northeastern Taiwan from pollen and diatom analysis of lake sediments. *Journal of Asian Earth Sciences* 114: 447–456.
- Wang L, Li J, Lu H et al. (2012a) The East Asian winter monsoon over the last 15,000 years: Its links to high-latitudes and tropical climate systems and complex correlation to the summer monsoon. *Quaternary Science Reviews* 32: 131–142.
- Wang T, Surge D and Mithen S (2012b) Seasonal temperature variability of the Neoglacial (3300–2500BP) and Roman Warm Period (2500–1600BP) reconstructed from oxygen isotope ratios of limpet shells (*Patella vulgata*), Northwest Scotland. *Palaeogeography, Palaeoclimatology, Palaeoecology* 317–318: 104–113.
- Weltje GJ, Bloemsma MR, Tjallingii R et al. (2015) Prediction of geochemical composition from XRF core scanner data: A new multivariate approach including automatic selection of calibration samples and quantification of uncertainties. In: Croudace IW and Rothwell RG (eds) *Micro-XRF Studies of Sediment Cores: Applications of A Non-Destructive Tool for the Environmental Sciences*. Dordrecht: Springer Netherlands, pp.507–534.
- Wu B, Zhang R and D’Arrigo R (2006) Distinct modes of the East Asian winter monsoon. *Monthly Weather Review* 134(8): 2165–2179.
- Xiang R, Yang Z, Saito Y et al. (2006) East Asia winter monsoon changes inferred from environmentally sensitive grain-size component records during the last 2300 years in mud area southwest off Cheju Island, ECS. *Science in China Series D* 49(6): 604–614.
- Xiao J, Chang Z, Si B et al. (2008) Partitioning of the grain-size components of Dali Lake core sediments: Evidence for lake-level changes during the Holocene. *Journal of Paleolimnology* 42(2): 249–260.
- Xiao J, Fan J, Zhai D et al. (2015) Testing the model for linking grain-size component to lake level status of modern clastic lakes. *Quaternary International* 355: 34–43.
- Yamamoto M, Yamamuro M and Tada R (2000) Late Quaternary records of organic carbon, calcium carbonate, and biomarkers from Site 1016 off Point Conception, California margin. *Proceedings of the Ocean Drilling Program, 167 Scientific Results*. The Program 167: 183–194.

- Yamoah KA, Callac N, Chi Fru E et al. (2016) A 150-year record of phytoplankton community succession controlled by hydroclimatic variability in a tropical lake. *Biogeosciences* 13(13): 3971–3980.
- Yang K, Hua W and Hu Q (2020) A multi-model analysis of the East Asian monsoon changes in the Medieval Climate Anomaly and Little Ice Age. *International Journal of Climatology* 40(12): 5084–5097.
- Yang T-N, Lee T-Q, Meyers PA et al. (2011) The effect of typhoon induced rainfall on settling fluxes of particles and organic carbon in Yuanyang Lake, subtropical Taiwan. *Journal of Asian Earth Sciences* 40(6): 1171–1179.
- Yang W, Zhou X, Xiang R et al. (2015) Reconstruction of winter monsoon strength by elemental ratio of sediments in the East China Sea. *Journal of Asian Earth Sciences* 114: 467–475.
- Yen MC and Chen TC (2000) Seasonal variation of the rainfall over Taiwan. *International Journal of Climatology* 20(7): 803–809.
- Zhang R-H (2015) Natural and human-induced changes in summer climate over the East Asian monsoon region in the last half century: A review. *Advances in Climate Change Research* 6(2): 131–140.
- Zhang R, Sumi A and Kimoto M (1996) Impact of El Niño on the east Asian monsoon. *Journal of the Meteorological Society of Japan. Ser. II* 74(1): 49–62.
- Zhang X, Jin L and Li N (2015) Asynchronous variation in the East Asian winter monsoon during the Holocene. *Journal of Geophysical Research: Atmospheres* 120(11): 5357–5370.
- Zhou W, Zheng Y, Meyers PA et al. (2010) Postglacial climate-change record in biomarker lipid compositions of the Hani peat sequence, Northeastern China. *Earth and Planetary Science Letters* 294(1–2): 37–46.
- Zhou X, Sun L, Huang W et al. (2012) Precipitation in the Yellow River drainage basin and East Asian monsoon strength on a decadal time scale. *Quaternary Research* 78(3): 486–491.